We are IntechOpen, the world's leading publisher of Open Access books Built by scientists, for scientists

4,800
Open access books available

122,000
International authors and editors

135M
Downloads

Our authors are among the

154
Countries delivered to

TOP 1%
most cited scientists

12.2%
Contributors from top 500 universities

CLARIVATE ANALYTICS BOOK CITATION INDEX INDEXED

WEB OF SCIENCE™

Selection of our books indexed in the Book Citation Index in Web of Science™ Core Collection (BKCI)

Interested in publishing with us?
Contact book.department@intechopen.com

Numbers displayed above are based on latest data collected.
For more information visit www.intechopen.com

5

Influence of Horizontal Temperature Gradients on Convective Instabilities with Geophysical Interest

H. Herrero, M. C. Navarro and F. Pla
Universidad de Castilla- La Mancha
Spain

1. Introduction

Since Bénard's experiments on convection and Rayleigh's theoretical work in the beginning of the twentieth century (1)-(2), many experimental, theoretical and numerical works related to Rayleigh-Bénard convection have been done (3)-(10) and different problems have been posed depending on what is to be modelled. Classically, heat is applied uniformly from below and the conductive solution becomes unstable for a critical vertical gradient beyond a certain threshold.

A setup for natural convection more general than that of uniform heating consists of including a non-zero horizontal temperature gradient which may be either constant or not (11)-(29).

In those problems a clear difference is marked by the fact that the fluid is simply contained (11)-(19), where stationary and oscillatory instabilities appear depending on the multiple parameters present in the problem: properties of the fluid, surface tension effects, heat exchange with the atmosphere, aspect ratio, dependence of viscosity with temperature, etc., and the case where the fluid can flow throughout the boundaries (29), where vortical solutions can appear reinforcing the relevance of convective mechanisms for the generation of vertical vortices very similar to those found for some atmospheric phenomena as dust devils or hurricanes (29)-(31).

The case where the fluid is simply contained displays stationary and oscillatory instabilities. This problem has been treated from different points of view: experimental (11)-(18) and theoretical, both with semiexact (20)-(21) and numerical solutions (40)-(28). This case contains applications to mantle convection when the viscosity is large (45; 52) or it depends on temperature (19).

There are not experiments yet for the case where a flow throughout the boundaries is allowed, only observations of atmospheric phenomena (30; 33; 34; 36; 37), and theoretic numerical results (29; 31).

In this work we will review this physical problem, focusing on the latest problems addressed by the authors on this topic, where a non-uniform heating is considered in different geometrical configurations, and we will show the relevant results obtained, some of them in the context of interesting atmospheric and geophysical phenomena (30; 36; 37).

2. Theoretical formulation of the problem

The physical set-up (see figure 1) consists of a horizontal fluid layer in a rectangular domain (19; 45) or a cylindrical annulus (18; 25; 28) between two vertical walls at $r = a$ and $r = a + l$. The depth of the domain is d (z coordinate). At $z = 0$ the imposed temperature gradient takes the value $T_{\max}$ at a and the value $T_{\min}$ at the outer part $(a + l)$. The upper surface is at temperature $T = T_0$. We define $\triangle T_v = T_{\max} - T_0$, $\triangle T_h = T_{\max} - T_{\min}$ and $\delta = \triangle T_h / \triangle T_v$.

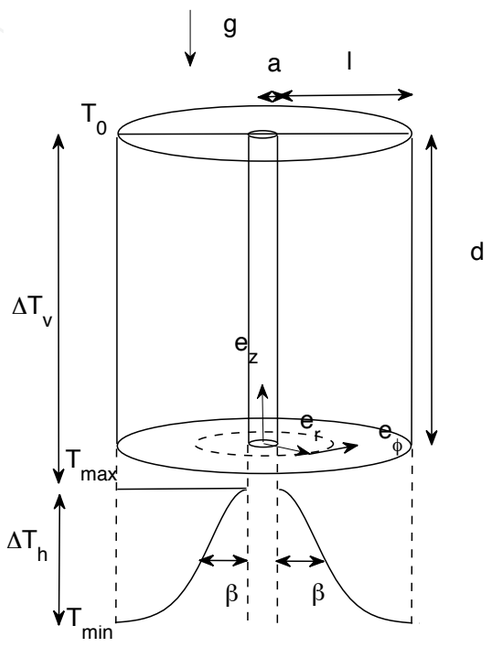

Fig. 1. Physical setup for the cylindrical annulus.

From now on we will consider an annular domain, therefore cylindrical coordinates will be used in the following. The formulation in a rectangular domain and coordinates would be similar. In the governing equations, $\mathbf{u} = (u_r, u_\phi, u_z)$ is the velocity field, T is the temperature, p is the pressure, r is the radial coordinate, and t is the time. They are expressed in dimensionless form after rescaling: $\mathbf{r}' = \mathbf{r}/d$, $t' = \kappa t/d^2$, $\mathbf{u}' = d\mathbf{u}/\kappa$, $p' = d^2 p/\left(\rho_0 \kappa \nu\right)$, $\Theta = \left(T - T_0\right)/\triangle T_v$. Here $\mathbf{r}$ is the position vector, κ the thermal diffusivity, ν the kinematic viscosity of the liquid, and ρ_0 the mean density at temperature T_0. The domain is $[\bar{a}, \bar{a} + \Gamma] \times [0, 1] \times [0, 2\pi]$ where $\Gamma = l/d$ is the aspect ratio and $\bar{a} = a/d$.
The system evolves according to the mass balance, energy conservation and momentum equations, which in dimensionless form (with primes now omitted) are,

$$\nabla \cdot \mathbf{u} = 0, \tag{1}$$

$$\partial_t \Theta + \mathbf{u} \cdot \nabla \Theta = \nabla^2 \Theta, \tag{2}$$

$$\partial_t \mathbf{u} + \left(\mathbf{u} \cdot \nabla\right) \mathbf{u} = Pr \left(-\nabla p + \nabla^2 \mathbf{u} + R\Theta \mathbf{e}_z\right), \tag{3}$$

where the operators and fields are expressed in cylindrical coordinates and the Oberbeck-Boussinesq approximation has been used (25), i.e. density is constant except in the term of gravity, where a linear dependence on temperature is considered. Here $\mathbf{e}_z$ is the unit vector in the z direction. The following dimensionless numbers have been introduced: the Prandtl number $Pr = \nu/\kappa$, and the Rayleigh number $R = g\alpha\triangle T d^3/\kappa\nu$, which represents the effect of buoyancy and in which α is the thermal expansion coefficient and g the gravitational acceleration. In the case of variable viscosity the laplacian operator in Eq. (3) takes the form $\mathrm{div}\left(\frac{\nu(\Theta)}{\nu_0}\cdot\left(\nabla\mathbf{u}+(\nabla\mathbf{u})^t\right)\right)$, where $\nu(\Theta)=\nu_0 e^{-\eta R\Theta}$.

2.1 Contained fluid

Regarding boundary conditions, several conditions can be considered such as that one where flow through the boundaries is not permitted. For instance at the lateral walls $r = \bar{a}$ and $r = \bar{a}+\Gamma$ the velocity is zero and an insulating wall is considered,

$$u_r = u_\phi = \partial_r u_z = \partial_r\Theta = 0, \ \text{ on } \ r=\bar{a} \ \text{ and } \ r=\bar{a}+\Gamma. \tag{4}$$

On the top surface, the vertical velocity is zero, the normal derivatives of the rest of components of the velocity are zero and the temperature is $T = T_0$, that after rescaling become,

$$\partial_z u_r = \partial_z u_\phi = u_z = \Theta = 0, \ \text{ on } \ z=1, \tag{5}$$

and at the bottom

$$u_r = u_\phi = u_z = 0, \ \text{ on } \ z=0. \tag{6}$$

For temperature at the bottom we consider a constant horizontal temperature difference, i.e. a linear profile. Here the horizontal temperature gradient appears,

$$\Theta = \theta^1(r) \quad \text{on } \ z=0. \tag{7}$$

with $\theta^1(r) = 1 - r\delta/\Gamma$ and a second order polynomial which matches the linear profile such that $\partial_r\theta^1(r) = 0$ on $r = \bar{a}$ and $r = \bar{a}+\Gamma$.
The dimensionless equations and boundary conditions contain five external parameters: R, Γ, Pr, δ, and η.

2.2 Not contained fluid

Regarding boundary conditions, several conditions can be considered like allowing flow through the boundaries. At the lateral inner wall $r = \bar{a}$ the velocity is zero and an insulating wall is considered,

$$u_r = u_\phi = u_z = \partial_r\Theta = 0, \ \text{ on } \ r=\bar{a}. \tag{8}$$

At $r = \bar{a}+\Gamma$, the lateral outer wall, a constant radial velocity is assumed and an insulating wall is considered,

$$\partial_r u_r = \partial_r u_\phi = \partial_r u_z = \partial_r\Theta = 0, \ \text{ on } \ r=\bar{a}+\Gamma. \tag{9}$$

On the top surface, the velocity is zero and the temperature is $T = T_0$, that after rescaling become,

$$u_r = u_\phi = u_z = \Theta = 0, \ \text{ on } \ z=1, \tag{10}$$

and at the bottom

$$u_r = \partial_z u_\phi = u_z = 0, \text{ on } z = 0. \tag{11}$$

For temperature at the bottom we consider a variable horizontal temperature gradient through imposing a Gaussian profile as in Ref. (28),

$$\Theta = 1 - \delta(e^{(\frac{1}{\beta})^2} - e^{(\frac{1}{\beta} - (\frac{r-\bar{a}}{\Gamma})^2 \frac{1}{\beta})^2})/(e^{(\frac{1}{\beta})^2} - 1) \text{ on } z = 0. \tag{12}$$

The dimensionless equations and boundary conditions contain five external parameters: R, Γ, Pr, δ, and β.

3. Metodology: search for solutions and their linear stability

We look for stationary axisymmetric solutions of the problem, then, the equations to be solved are

$$\nabla^* \cdot \mathbf{u} = 0, \tag{13}$$

$$\mathbf{u} \cdot \nabla^* \Theta = \nabla^{*2} \Theta, \tag{14}$$

$$(\mathbf{u} \cdot \nabla^*)\, \mathbf{u} = Pr \left(-\nabla^* p + \nabla^{*2} \mathbf{u} + R\Theta \mathbf{e}_z \right), \tag{15}$$

where $\nabla^* = (\partial_r, 0, \partial_z)$, together with the corresponding boundary conditions.
The time independent solution $U^b(r,z)$ to the stationary problem obtained from equations (1)-(3) by eliminating the time dependence, is called basic state. It is a non-conductive state ($\mathbf{u} \neq 0$) as soon as $\delta \neq 0$. The basic state is considered to be axisymmetric and therefore depends only on $r - z$ coordinates (i.e. all ϕ derivatives are zero). The velocity field of the basic flow is restricted to $\mathbf{u} = (u_r, u_\phi = 0, u_z)$.
A linear stability analysis of the stationary solutions is performed. Fixed $(\Gamma, \delta, Pr, \beta)$, the solution $U(r,z,t) = (\mathbf{u}, \Theta, p)(r,z,t)$ of (1)-(3) at given R is expressed as

$$U(r,z,t) = U^b(r,z) + \tilde{U}(r,z) e^{ik\phi + \lambda t}, \tag{16}$$

where $U^b(r,z)$ is the base flow for the given $(R, \Gamma, \delta, Pr, \beta)$ and $\tilde{U}(r,z)$ refers to the perturbation. We have considered Fourier mode expansions in the angular direction, because along it boundary conditions are periodic. Introducing (16) into the full system (1)-(3) and linearizing the resulting system, the following eigenvalue problem in λ is obtained:

$$\nabla^k \cdot \tilde{U} = 0, \tag{17}$$

$$\lambda \tilde{\Theta} + \tilde{U} \cdot \nabla^k \Theta^b + U^b \cdot \nabla^k \tilde{\Theta} = (\nabla^k)^2 \tilde{\Theta}, \tag{18}$$

$$\lambda \tilde{U} + \left(\tilde{U} \cdot \nabla^k \right) U^b + \left(U^b \cdot \nabla^k \right) \tilde{U} = Pr \left(-\nabla^k \tilde{p} + (\nabla^k)^2 \tilde{U} + R\tilde{\Theta} \mathbf{e}_z \right), \tag{19}$$

where $\nabla^k = (\partial_r, ik, \partial_z)$, with the corresponding boundary conditions.
The instability is achieved when the real part of the eigenvalue with maximum real part, $\lambda_{\max}(R)$, changes from a negative value to a positive one as R increases, for a specific wave

number k. The critical value of R for which $\lambda_{\max}(R,k) = 0$ is denoted by R_c and the critical wave number, minimum k for which the bifurcation occurs, by k_c.

3.1 Numerical methods

The numerical method is described in detail and tested in Refs. (25; 28). The nonlinearities in the basic state problem are solved with a Newton method. Each step of the Newton method and the linear stability analysis have been numerically solved with a Chebyshev collocation method as explained in Refs. (28; 39; 48). The problem is posed in the primitive variables formulation, and the use of the same order approximations for velocity and pressure in the Chebyshev collocation procedure introduces spurious modes for pressure that are solved by adding convenient boundary conditions (43; 44). In the resulting linear problems any unknown field $\mathbf{x}$ is expanded in Chebyshev polynomials

$$\mathbf{x}^{LN} = \sum_{l=0}^{L-1} \sum_{n=0}^{N-1} a_{ln}^{\mathbf{x}} T_l(r) T_n(z). \tag{20}$$

The corresponding expansions for the four different fields are introduced into the Newton linearized version of equations (13)-(15) and the corresponding boundary conditions and evaluated at the Chebysehv Gauss-Lobatto collocation points (r_j, z_i),

$$r_j = \cos\left(\left(\frac{j-1}{L-1} - 1\right)\pi\right), \quad j = 1, ..., L. \tag{21}$$

$$z_i = \cos\left(\left(\frac{i-1}{N-1} - 1\right)\pi\right), \quad i = 1, ..., N. \tag{22}$$

Some care is necessary in the evaluation rules at the boundaries as explained in Refs. (28; 48). At each iteration of the Newton method a linear system of the form $AX = B$ is derived, where X is a vector containing $P = 4 \times L \times N$ unknowns and A is a full rank matrix of order $P \times P$. This can be solved with standard routines. The algorithm starts with an approximation to the solution $\mathbf{x}^{0,LN}$ and the iteration procedure is applied until the stop criterion $||\mathbf{x}^{s+1,LN} - \mathbf{x}^{s,LN}|| < 10^{-9}$ is satisfied.

The same discretization is used for the eigenvalue problem (17)-(19) with the corresponding boundary conditions. In this way it is transformed into its discrete form by expanding the perturbations in a truncated series of Chebyshev polynomials (20) as performed for the basic state. The evaluation rules are detailed in Ref. (48). Therefore, the eigenvalue problem in its discrete form is,

$$Cw = \sigma Bw, \tag{23}$$

where w is a vector which contains Q unknowns and C and B are $Q \times Q$ matrices, with $Q = 5 \times L \times N$.

QZ or Arnoldi algorithms are used to solve the eigenvalue problem (42). σ are the eigenvalues and w are coefficients in the Chebyshev basis of the corresponding eigenfunctions.

The discrete eigenvalue problem (23) has a finite number of eigenvalues σ_i. The stability condition must now be imposed upon $\sigma_{\max}$ where $\sigma_{\max} = \max(\mathrm{Re}(\sigma_i))$, bearing in mind

that if $\sigma_{\max} < 0$ the stationary state is stable while if $\sigma_{\max} > 0$ the stationary state becomes unstable. The control or bifurcation parameter is the Rayleigh number R. For fixed values of the parameters, in those cases Γ, Pr, δ, β or η, the critical values are the minimum value of R_c for which there exists a value of k, k_c, such that $\sigma(R_c, k_c) = 0$.
In order to test convergence of the method we include, as an example, the calculation of the critical value of the bifurcation parameter, R_c, and the critical wave number, k_c, for different order expansions in the Chebyshev approximation in the contained fluid case. And we benchmark the method and code to ensure the correctness of the results. Table 1 shows these results for the contained fluid case. When the orders L and N are increased, the critical values tend to a determined value, convergence is very good and for $L = 24$ and $N = 14$ the results are sufficiently accurate, in fact they are exact to the thousandth. The values $L = 24$ and $N = 14$ can be considered in the computations. In a convergence test comparing the critical R_c obtained at different order expansions, the relative difference between the expansions at 26×18 and 24×16 is found to be less than 10^{-4}. There are three significant digits in this calculation. The benchmarking of the method can be done with results in Ref. (48). The critical wave number for $\Gamma = 2.936$, $\eta = 0.0862$ and $\delta = 0$ is $k_c = 0$, so for these values of the parameters the results reported in Ref. (48) are recovered. For this value of the aspect ratio the bifurcation corresponds to a mode 2 in the x direction and the bifurcation takes place at the same value $R_c = 73.5$.

	$N = 12$	$N = 14$	$N = 16$	$N = 18$
$L = 14$	(2.5, 1203.91)	(2.5, 1210.00)	(2.5, 1212.73)	(2.5, 1208.70)
$L = 16$	(2.5, 1220.00)	(2.5, 1214.00)	(2.5, 1214.92)	(2.5, 1214.94)
$L = 18$	(2.5, 1220.10)	(2.5, 1225.00)	(2.5, 1224.92)	(2.5, 1224.07)
$L = 20$	(2.5, 1220.10)	(2.5, 1224.15)	(2.5, 1224.90)	(2.5, 1224.90)
$L = 22$	(2.5, 1220.20)	(2.5, 1224.92)	(2.5, 1224.92)	(2.5, 1224.92)
$L = 24$	(2.5, 1220.20)	(2.5, 1225.00)	(2.5, 1225.00)	(2.5, 1224.92)
$L = 26$	(2.5, 1220.20)	(2.5, 1225.00)	(2.5, 1224.92)	(2.5, 1224.92)

Table 1. $(k_c,\ R_c)$ for different order expansions in L and N in the Chebyshev expansion (20) for a 3D fluid with constant viscosity, $\eta = 0$, aspect ratio $\Gamma = 2.936$ and $\delta = 0.1$.

4. Numerical solutions with geophysical interest

4.1 Contained fluid

In references of small cells the case of large viscosity (or Prandlt number) could be considered as an approximation to mantle convection. The largest value of Prandlt number considered in the experiments is $Pr = 60$ in Ref. (52), in this case boundary layer waves are observed. Numerical results with infinite Pr number are reported in (45). In this case only stationary patterns of rolls perpendicular to the temperature gradient are observed. Also it is of interest the case of variable viscosity dependent on temperature, this case is plenty of references, but all of them consider homogeneous heating without horizontal temperature gradients (35; 36; 47). The only reference in which those gradients are taken into account in a variable viscosity case is (19). Some numerical solutions obtained in the case considered in Ref. (19) are presented in figure 2 at infinite Pr number, aspect ratio $\Gamma = 2.936$, $\eta = 0.0862$, $R = 72.650$ and

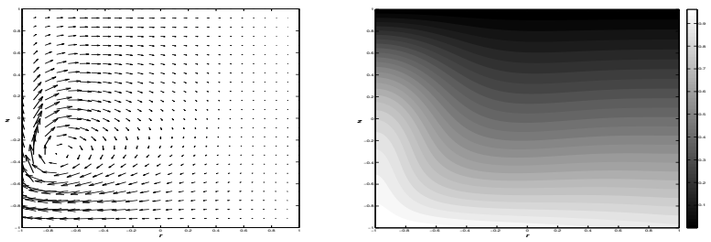

Fig. 2. Basic state for $\Gamma = 2.936$, $\eta = 0.0862$, $\delta = 0.1$ and $R = 72.65$. On the left velocity field $\mathbf{u}$. On the right Isotherms of temperature Θ.

$\delta = 0.1$. Figure 2 shows that the structure of the velocity field is more localized close to the zone where the temperature is higher, i.e, at $r = -1$. The presence of the horizontal gradient generates convective basic states, that were conductive without the horizontal gradients. In Ref. (19) it is shown the fluid motion is produced in the region where viscosity is lower.
Regarding the instabilities, in the case of large Γ the influence of the horizontal temperature gradient is considerable, the problem is nearly two-dimensional (2D) in the uniform heating case, but it is three-dimensional (3D) with the horizontal temperature gradient. Figure 3 shows the growing mode or eigenfunction in the case $\Gamma = 2.936$, $\delta = 0$ and $\eta = 0.0862$, the critical wave number in this case is $k_c = 0$, so a 2D structure appears after the bifurcation. Figure 4 shows the growing mode or eigenfunction in the same case as before, but with horizontal gradient $\delta = 0.1$, the critical wave number in this case is $k_c = 1.7$, so a 3D structure appears after the bifurcation. Also we can observe from figures 3 and 4 that the bifurcating pattern is more structured in the $r - z$ plane for $\delta = 0$ and becomes more structured in the $y - z$ plane for $\delta \neq 0$. Hence, a horizontal temperature gradient gives rise to thermal plumes which bifurcate to totally 3D structures.

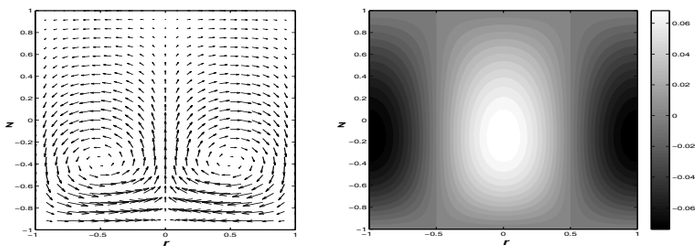

Fig. 3. Growing mode or eigenfunction at the instability threshold for $\Gamma = 2.936$, $\delta = 0$, $\eta = 0.0862$ and $R_c = 72.504$. On the left velocity field $\mathbf{u}$. On the right Isotherms of temperature Θ.

4.2 Not contained fluid

This case is plenty of references of direct simulations solving numerically the partial differential equations (31; 34). But under the instability or bifurcation perspective the case in which the fluid can flow through the boundaries is only treated in reference (29). In that paper we show that a vortical structure appears after a stationary bifurcation of a state without angular velocity.

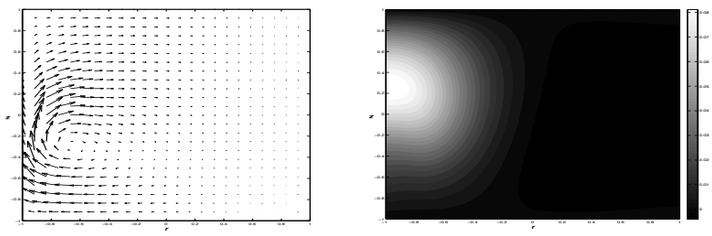

Fig. 4. Growing mode or eigenfunction at the instability threshold for $\Gamma = 2.936$, $\delta = 0.1$, $\eta = 0.0862$ and $R_c = 72.650$. On the left velocity field $\mathbf{u}$. On the right Isotherms of temperature Θ.

A numerical solution obtained in the problem considered in Ref. (29) is presented in figure 5. Figure 5 shows the profiles of temperature, pressure and velocity components corresponding to the clockwise vortex for $Pr = 0.7$, $\Gamma = 0.5$ and $\delta = 10$ at $R = 4367$. This vortex appears after a bifurcation of a basic state with zero azimuthal velocity (see Ref. (29)). The main feature of the new steady flow emerging from the convective instability with $k_c = 0$ and $\tilde{u}_\phi \neq 0$ is a non-zero azimuthal velocity component. The fluid inside the annulus begins to move in the azimuthal direction, rotating around the inner cylinder.
The linear stability analysis of the vortical structures shows that there is a wide range of parameters for which this state is stable.
The track of a particle in the vortex can be obtained by integrating the evolution of the element of fluid which follows the velocity field,

$$\frac{dr}{dt} = u_r(r,z), \tag{24}$$

$$\frac{d\phi}{dt} = u_\phi(r,z), \tag{25}$$

$$\frac{dz}{dt} = u_z(r,z). \tag{26}$$

In our simulations we observe a spiral upward motion of the particle around the inner cylinder, which implies a transport of mass in the azimuthal direction. Starting from below, the particle goes up, moves towards the inner cylinder and rotates around it. The combination of these movements gives the spiral trajectory shown in figure 6, where the trajectory of a particle in the fluid is presented for $\Gamma = 0.5$, $\delta = 10$ and $R = 4367$ at two different initial conditions. Starting from a point close to the bottom plate but near the inner cylinder, where the effect of u_z is stronger than the effect of u_ϕ, the particle goes up very fast without much turning around the inner cylinder. This can be appreciated in figure 6 a) where the starting point considered is $(r = 0.085, z = 0.05, \phi = 0)$ in $[0.06, 0.56] \times [0, 1] \times [0, 2\pi]$. When the particle reaches the upper part of the structure it describes wider circles around the inner cylinder as u_r becomes positive and u_z is very small at those levels (see figure 5). Figure 6 b) shows the effect of localizing the starting point further from the inner cylinder, e.g. at $(r = 0.31, z = 0.05, \phi = 0)$. In this case, the effect of u_ϕ is stronger and the spiral up motion of the particle starts as soon as the particle begins to move.

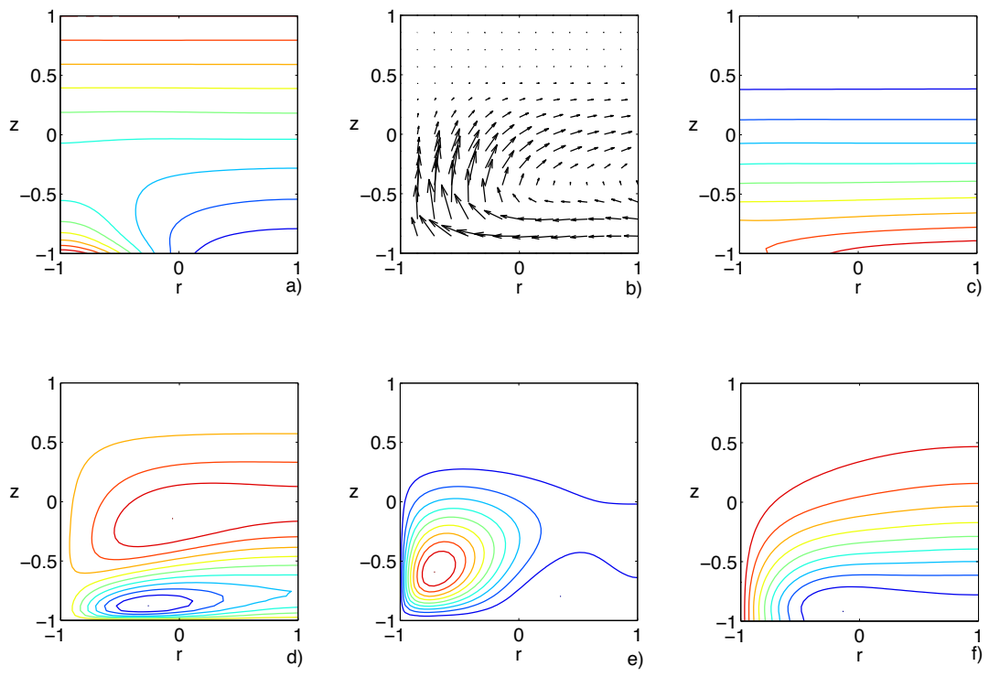

Fig. 5. Clockwise vortex at $\Gamma = 0.5$, $\delta = 10$ and $R = 4367$. a) Isotherms of Θ; b) meridional velocity (u_r, u_z); c) contour plot of the pressure p ; d) contour plot of the radial velocity component u_r; e) contour plot of the vertical velocity component u_z; f) contour plot of the azimuthal velocity component u_ϕ. The contours correspond to equally spaced values within their ranges of [-9:1] for Θ, [-0.02:20.4] $\cdot 10^3$ for p, [-9.3:4.3] for u_r, [-0.6:14.5] for u_z and [-26.1:0] for u_ϕ. The pressure p is determined up to a constant.

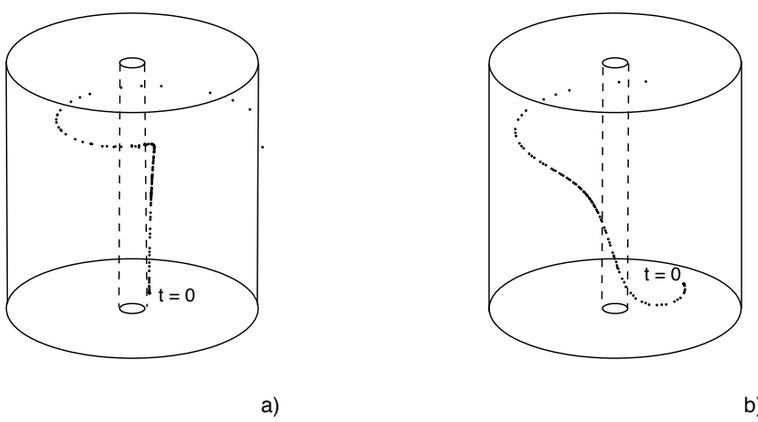

Fig. 6. Track of a particle in the fluid for the stable clockwise vortex. The values of the parameters are $\Gamma = 0.5$, $\delta = 10$ and $R = 4367$. a) Starting point at $(r = 0.085, z = 0.05, \phi = 0)$; b) starting point at $(r = 0.31, z = 0.05, \phi = 0)$.

5. Discusion

5.1 Contained fluid

Regarding the numerical solutions found in this case, the horizontal temperature gradient generates convective states and tends to concentrate motion near the warmer wall. This fact coincides with experiments in Refs. (38; 40; 41) and is consistent with previous numerical results reported in (27; 45). The temperature dependent viscosity localizes motion near the region of lower viscosity, i.e., the bottom plate. This also coincides with experiments in Refs. (36; 46; 49) and numerical results in Ref. (48). It is remarkable that the horizontal temperature gradient favours a threedimensional structure after the bifurcation, while the pattern continues being axisymmetric after the bifurcation in the only vertical gradient case.

5.2 Not contained fluid

As detailed in Ref. (48) we found qualitative similarities between the vortical structures computed numerically and some meteorological phenomena such as dust devils and cyclones. One of the main characteristics of dust devils is a low-pressure region in the center of the dust devil which coincides with the dust devil's warm core (33). This is also observed in our numerical vortices (see figure 5 c). Regarding temperature, in dust devils, the maximum temperature deviation from the environment temperature (i.e. the temperature furthest from the dust devil center) occurs at the lowest levels. This feature is observed in the temperature profile of our vortices.

The experimental measures provided in Ref. (33) show that there is radial inflow at the lower levels of the dust devil and radial outflow in the upper levels. It is also shown that the vertical velocity reaches highest values and then falls off rapidly as the radius is increased. These features are appreciated in the profile of u_r and u_z shown in figures 5 d) and e).

The trajectory of particles around the inner cylinder described in this section appears to be very similar to the trajectory of particles of air (or dust) in a dust devil, characterized by a spiral up motion (33).

Other more complex meteorological phenomena such as cyclones also present these structural characteristics. It is known that the center (eye) of a cyclone is the area of lowest atmospheric pressure in the region, which corresponds to a warm core in some kind of cyclones (e.g. tropical and mesoscale) (31; 34). This coincides with that observed in figures 5 a) and 5 b). Regarding the motion in cyclones, it is observed the inward flow next to the surface, strong upward motion in the eyewall and outflow in a layer near the top of the storm (31; 34). This characteristic is described in the combined effect of the radial and vertical velocity components observed in our vortices as pointed out above (see figures figures 5 c, d) and e)). In cyclones, a counter-clockwise motion (clockwise in the southern hemisphere) is observed around the center of the storm, stronger just above the surface in a ring around the center and sligther as we go up from the surface (31; 34). That coincides with the effect of the azimuthal velocity component observed in the vortices we have computed numerically responsible for the movement of the particles around the inner cylinder.

6. Conclusions

In this work we have reviewed the influence of horizontal temperature gradients on convective instabilities, focusing on results with geophysical interest.

We have distinguished two cases, a first one where the fluid is simply contained in a domain, and a second one where the fluid can flow throughout the boundaries.
In the first case three subcases can be grouped. The case corresponding to small cells and small *Pr* number displays stationary and oscillatory instabilities depending on the multiple parameters present in the problem: properties of the fluid, surface tension effects, heat exchange with the atmosphere, aspect ratio, dependence of viscosity with temperature, etc. This problem has been treated from experimental, theoretical and numerical points of view. The cases corresponding to small cells and large or infinite *Pr* number are closer to mantle convection. Boundary layer waves are observed in experiments and 3D stationary patterns of rolls perpendicular to the temperature gradient appear numerically. Finally for the case of infinite *Pr* number with temperature dependent viscosity, the closest to mantle convection, 3D stationary patterns concentrated in the region of lower viscosity and waves for larger values of the *R* number appear. Summarizing, horizontal temperature gradients favour the presence of waves and the totally three dimensional patterns.
The problem where the fluid can flow throughout the boundaries has been treated usually as direct numerical simulations. For the first time it has been studied under the perspective of instabilities or bifurcations in Ref. (29). In this reference vortical solutions, very similar to those found for some atmospheric phenomena such as dust devils or hurricanes, appear after a stationary bifurcation. This is a powerfull and simple explanation of those atmospheric phenomena as an instability.

7. Acknowledgements

This work was partially supported by Research Grant MICINN (the Government of Spain) MTM2009-13084 and CCYT (Junta de Comunidades de Castilla-La Mancha) PAI08-0269-1261, which include RDEF funds.

8. References

[1] H. Bénard *Rev. Gén. Sci. Pures Appl.* 11, 1261 (1900).
[2] Lord Rayleigh. On convective currents in a horizontal layer of fluid when the temperature is on the under side. Phil. Mag. 32, pp. 529-46 (1916).
[3] S. Chandrasekhar. *Hydrodynamic and Hydromagnetic Stability*. Dover Publications, New York, 1981.
[4] E. Bodenschatz, J. R. de Bruyn, G. Ahlers, and D. S. Cannell. Transitions between patterns in thermal convection. *Phys. Rev. Lett.* 67, 3078-3081, 1991.
[5] S.W Morris, E. Bodenschatz, D. S. Cannell and G. Ahlers. Spiral defect chaos in large aspect ratio Rayleigh-Bénard convection. *Phys. Rev. Lett.* 71, 2026-2029, 1993.
[6] E.L. Koschmider. Bénard Cells and Taylor Vortices. Cambridge University Press, 1993.
[7] M. Assenheimer, V. Steinberg, "Transition between spiral and target states in Rayleigh-Bénard Convection". *Nature* 367 (6461) 345 (1994).
[8] E. Bodenschatz, W. Pesch and G. Ahlers. Recent developments in Rayleigh-Bénard convection. *Annual Review of Fluid Mechanics* 32, 709-778, 2000.
[9] B. B. Plapp, D. A Egolf, E. Bodenschatz and W. Pesch. Dynamics and selection of giant spirals in Rayleigh-Bénard convection. *Phys. Rev. Lett.* 81, 5334-5337, 1998.

[10] S. Rüdiger and F. Feudel. Pattern formation in Rayleigh Bénard convection in a cylindrical container. *Phys. Rev. E* 62, 4927-4931, 2000.
[11] A.B. Ezersky, A. Garcimartín, J. Burguete, H.L. Mancini and C. Pérz-García, "Hydrothermal waves in Marangoni convection in a cylindrical container." *Phys. Rev. E* 47, 1126 (1993).
[12] M.A. Pelacho and J. Burguete, "Temperature oscillations of hydrothermal waves in thermocapillary-buoyancy convection."*Phys. Rev. E* 59, 835 (1999).
[13] E. Favre, L. Blumenfeld and F. Daviaud, "Instabilities of a liquid layer locally heated on its free surface."*Phys. Fluids* 9, 1473 (1997).
[14] N. Garnier and A. Chiffaudel. "Two dimensional hydrothermal waves in an extended cylindrical vessel." *Eur. Phys. J. B* 19, 87 (2001).
[15] N. Garnier and C. Normand. "Effects of curvature on hydrothermal waves instability of radial thermocapillary flows." *C. R. Acad. Sci., Ser. IV* 2 (8) 1227 (2001).
[16] B.C. Sim, A. Zebib. "Effect of free surface heat loss and rotation on transition to oscillatory thermocapillary convection." *Phys. Fluids* 14 (1), 225 (2002).
[17] B.C. Sim, A. Zebib, D. Schwabe. "Oscillatory thermocapillary convection in open cylindrical annuli. Part 2. Simulations."*J. Fluid Mech.* 491, 259 (2003).
[18] S. Hoyas, A.M. Mancho, H. Herrero, N. Garnier, A. Chiffaudel. "Bénard-Marangoni convection in a differentially heated cylindrical cavity" *Phys. Fluids*, 17, 054104 (2005).
[19] F. Pla and H. Herrero "Effects of non uniform heating in a variable viscosity Rayleigh-Bénard problem". *Theoretical and Computational Fluid Dynamics*, DOI: 10.1007/s00162-010-0189-3, 2010.
[20] M. K. Smith and S. H. Davis, "Instabilities of dynamic thermocapillary layers. 1. Convective instabilities." *J. Fluid Mech.* 132, 119 (1983).
[21] De Saedeleer, C., Garcimartin, A., Chavepeyer, G., Platten, J.K., Lebon, G.: The instability of a liquid layer heated from the side when the upper surface is open to air. Phys. Fluids 8(3), pp. 670-676 (1996).
[22] A. M. Mancho, H. Herrero and J. Burguete, "Primary instabilities in convective cells due to non-uniform heating."*Phys. Rev E* 56, 2916 (1997).
[23] H. Herrero and A. M. Mancho "Influence of aspect ratio in convection due to non-uniform heating." *Phys. Rev E* 57, 7336 (1998).
[24] R.J. Riley and G.P. Neitzel, "Instability of thermocapillary-buoyancy convection in shallow layers. Part 1. Characterization os steady and oscillatory instabilities." *J. Fluid Mech* 359 , 143 (1998).
[25] S. Hoyas, H. Herrero and A.M. Mancho, "Thermal convection in a cylindrical annulus heated laterally." *J. Phys. A: Math and Gen.* 35, 4067 (2002).
[26] S. Hoyas, H. Herrero and A.M. Mancho, "Bifurcation diversity of dynamic thermocapillary liquid layers."*Phys. Rev. E*, 66, 057301 (2002).
[27] S. Hoyas, H. Herrero, A.M. Mancho, "Thermocapillar and thermogravitatory waves in a convection problem". *Theoretical and Computational Fluid Dynamics* 18, 2-4, 309 (2002).
[28] M. C. Navarro, A. M. Mancho and H. Herrero, "Instabilities in buoyant flows under localized heating."*Chaos* 17, 023105 (2007).
[29] M. C. Navarro, H. Herrero, "Vortex generation by a convective instability in a cylindrical annulus non homogeneously heated". *Physica D,* accepted (2011).

[30] N. O. Rennó, M. L. Burkett, M. P. Larkin, "A simple theory for dust devils". *J. Atmos. Sci.* 55 3244 (1998).
[31] K. A. Emanuel. *Divine wind.* Oxford University Press, Oxford, 2005.
[32] L. Battan, Energy of a dust devil, J. Meteor. 15 (1958) 235-237.
[33] P. C. Sinclair, The lower structure of dust devils, J. Atmos. Sci. 30 (1973) 1599-1619.
[34] K. A. Emanuel, Thermodynamic control of hurricane intensity, Nature 401 (1999) 665-669.
[35] Bercovici, D.: The generation of plate tectonics from mantle convection. Earth and Planetary Science Letters 205, pp. 107-121 (2003).
[36] Booker, J.R.: Thermal convection with strongly temperature-dependent viscosity. J. Fluid Mech. 76 (4), pp. 741-754 (1976).
[37] Bunge, H.P., Richards, M.A., Baumgardner, J.R.: Effects of depth-dependent viscosity on the platform of mantle convection. Nature 379, pp. 436-438 (1996).
[38] Burguete, J., Mokolobwiez, N., Daviaud, F., Garnier, N., Chiffaudel, A.: Buoyant-thermocapillary instabilities in extended layers subjected to a horizontal temperature gradient. Phys. Fluids 13, pp. 2773-2787 (2001).
[39] Canuto, C., Hussaini, M.Y., Quarteroni, A., Zang, T.A. Spectral Methods in Fluid Dynamics. Springer, Berlin (1988).
[40] Daviaud, F., Vince, J.M.: Traveling waves in a fluid layer subjected to a horizontal temperature gradient. Phys. Rev. E 48, pp. 4432-4436 (1993).
[41] De Saedeleer, C., Garcimartin, A., Chavepeyer, G., Platten, J.K., Lebon, G.: The instability of a liquid layer heated from the side when the upper surface is open to air. Phys. Fluids 8(3), pp. 670-676 (1996).
[42] Golub, G.F., Van Loan, C.F.: Matrix Computations. The Johns Hopkins University Press. Baltimore and London, (1996).
[43] Herrero, H., Mancho, A.M.: On pressure boundary conditions for thermoconvective problems. Int. J. Numer. Meth. Fluids 39, pp. 391-402 (2002).
[44] Herrero, H., Hoyas, S., Donoso, A., Mancho, A.M., Chacón, J.M., Portugues, R.F., Yeste, B.: Chebyshev Collocation for a Convective Problem in Primitive Variables Formulation. J. of Scientific Computing 18(3), pp. 315-328 (2003).
[45] Mancho, A.M., Herrero, H.: Instabilities in a laterally heated liquid layer. Phys. Fluids 12, pp. 1044-1051 (2000).
[46] Manga, M., Weeraratne, D., Morris, S.J.S.: *Boundary-layer thickness and instabilities in Bénard convection of a liquid with a temperature-dependent viscosity*, Phys. Fluids 13 (3), pp. 802-805 (2001).
[47] Moresi, L.N., Solomatov, V.S.: Numerical investigation of 2D convection with extremely large viscosity variations, Phys. Fluids, 7 (9), pp. 2154-2162 (1995).
[48] Pla, F., Mancho, A.M., Herrero, H.: Bifurcation phenomena in a convection problem with temperature dependent viscosity at low aspect ratio. Physica D, 238, pp. 572-580, (2009).
[49] Richter, F.M., Nataf, H.C., Daly, S.F.,: *Heat transfer and horizontally averaged temperature of convection with large viscosity variations*, J. Fluid Mech. 129, pp. 173-192 (1983).
[50] Trompert, R., Hansen, U.:Mantle convection simulations with rheologies that generate plate-like behaviour, Nature 395 (6703), pp. 686-689 (1998).

[51] Yanagawa, T.K.B., Nakada, M., Yuen, D.A.: A simplified mantle convection model for thermal conductivity stratification. Physics of the Earth and Planetary Interiors 146, pp. 163-177 (2004).

[52] A.B. Ezersky, A. Garcimartín, J. Burguete, H.L. Mancini and C. Pérez García. *Hydrothermal waves in Marangoni convection in a cylindrical container*. Phys. Rev. E 47, pp. 1126-1131, 1993; A.B. Ezersky, A. Garcimartín, H.L. Mancini and C. Pérez García. *ibid*. 48, pp. 4414, 1993.

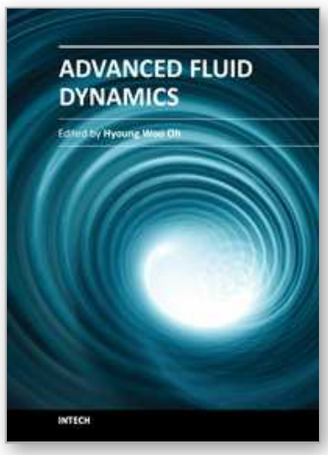

Advanced Fluid Dynamics

Edited by Prof. Hyoung Woo Oh

ISBN 978-953-51-0270-0
Hard cover, 272 pages
Publisher InTech
Published online 09, March, 2012
Published in print edition March, 2012

This book provides a broad range of topics on fluid dynamics for advanced scientists and professional researchers. The text helps readers develop their own skills to analyze fluid dynamics phenomena encountered in professional engineering by reviewing diverse informative chapters herein.

INTECH
open science | open minds

InTech Europe
University Campus STeP Ri
Slavka Krautzeka 83/A
51000 Rijeka, Croatia
Phone: +385 (51) 770 447
Fax: +385 (51) 686 166
www.intechopen.com

InTech China
Unit 405, Office Block, Hotel Equatorial Shanghai
No.65, Yan An Road (West), Shanghai, 200040, China
中国上海市延安西路65号上海国际贵都大饭店办公楼405单元
Phone: +86-21-62489820
Fax: +86-21-62489821

IntechOpen